

# HDTM: A Novel Model Providing Hydrostatic Delay and Weighted Mean Temperature for Real-Time GNSS Precipitable Water Vapor Retrieval

Luhong Li<sup>ID</sup>, Hongxing Zhang<sup>ID</sup>, Yunbin Yuan, Matthias Aichinger-Rosenberger<sup>ID</sup>, and Benedikt Soja<sup>ID</sup>

**Abstract**—Timely zenith hydrostatic delay (ZHD) and weighted mean temperature ( $T_m$ ) are critical for real-time GNSS precipitable water vapor (PWV) retrieval. However, for GNSS stations without collocated meteorological sensors, ZHD and  $T_m$  data are often inaccessible. Although atmospheric reanalysis offers an accurate alternative, its latency impedes real-time GNSS PWV retrieval. In this study, we propose a novel model, HDTM, capable of providing hourly updated ZHD and  $T_m$  forecast grids using freely available numerical weather predictions (NWPs), NCEP-GFS, and ECMWF-IFS. The HDTM model was validated over land and ocean regions in China, utilizing data from ERA5 reanalysis, 953 GNSS/meteorological stations, 64 radiosonde stations, and oceanic in situ pressure measurements. The results demonstrate that: 1) the HDTM model outperforms the traditional models, particularly in capturing the diurnal variations of ZHD and  $T_m$ , with ZHD root mean square (rms) errors of 3.2 mm (1.9 mm over oceans) and  $T_m$  rms error of 1.5 K; 2) PWV values retrieved using HDTM exhibit negligible discrepancies from those retrieved using in situ meteorological parameters, with a mean rms of 0.9 mm across China; and 3) in two extreme rainfall events, HDTM demonstrated superior accuracy in capturing ZHD and  $T_m$  and retrieved highly variable PWV with an rms of 1.1 mm. Overall, HDTM can provide high-quality ZHD and  $T_m$  forecasts under both stable and turbulent weather conditions, facilitating precise real-time GNSS PWV monitoring over both land and ocean without relying on collocated meteorological sensors.

Received 15 July 2024; revised 22 October 2024; accepted 14 November 2024. Date of publication 17 December 2024; date of current version 31 December 2024. This work was supported in part by the National Natural Science Foundation of China under Grant 42274043, in part by Wuhan Natural Science Foundation Exploration Program (Chen Guang Program) under Grant 2024040801020244, in part by the National Key Research and Development Program under Grant 2023YFA1009100, and in part by Wuhan Talents Plan (2023) and China Scholarship Council under Grant 202304910368. (Corresponding author: Hongxing Zhang.)

Luhong Li is with the State Key Laboratory of Geodesy and Earth's Dynamics, Innovation Academy for Precision Measurement Science and Technology, Chinese Academy of Sciences, Wuhan 430077, China, also with the College of Earth and Planetary Sciences, University of Chinese Academy of Sciences, Beijing 101408, China, and also with the Institute of Geodesy and Photogrammetry, ETH Zürich, 8093 Zürich, Switzerland (e-mail: li.luhong@whigg.ac.cn).

Hongxing Zhang and Yunbin Yuan are with the State Key Laboratory of Geodesy and Earth's Dynamics, Innovation Academy for Precision Measurement Science and Technology, Chinese Academy of Sciences, Wuhan 430077, China (e-mail: caszhx@whigg.ac.cn; yybgs@whigg.ac.cn).

Matthias Aichinger-Rosenberger and Benedikt Soja are with the Institute of Geodesy and Photogrammetry, ETH Zürich, 8093 Zürich, Switzerland (e-mail: maichinger@ethz.ch; soja@ethz.ch).

Digital Object Identifier 10.1109/TGRS.2024.3519428

**Index Terms**—Precipitable water vapor (PWV), real-time GNSS, severe rainfall, weighted mean temperature ( $T_m$ ), zenith hydrostatic delay (ZHD).

## I. INTRODUCTION

TIMELY sensing of atmospheric precipitable water vapor (PWV) is crucial for short-term severe weather predictions. PWV can be retrieved from GNSS-derived zenith tropospheric delays (ZTDs) with the aid of two auxiliary meteorological parameters: zenith hydrostatic delay (ZHD) and weighted mean temperature ( $T_m$ ) [1], [2].

The ZHD is used to separate the zenith wet delay (ZWD) from ZTD and can be accurately calculated using in situ pressure [3].  $T_m$  is employed to convert the ZWD to PWV and can be rigorously calculated by integrating a function of atmospheric profiles [1]. However, many GNSS stations are often unable to access collocated pressure and temperature parameters, especially for real-time applications. Thus, we can estimate the real-time GNSS ZTD but fail to obtain PWV synchronously due to a lack of timely ZHD and  $T_m$ .

Various methods have been proposed to obtain ZHD without co-located meteorological data, such as using interpolated data from nearby meteorological stations, numerical weather models (NWMs), and empirical models [4], [5], [6]. The accuracy may be degraded by the interpolated pressure data from a sparse meteorological network over complex terrains. NWM reanalysis data suffers from latency, which is not applicable for real-time practice [7], [8], [9]. The empirical models can provide various tropospheric parameters at any location over the globe, such as GPT3 and GZTD [10], [11], [12], [13], [14], but fail in capturing the short-term variations, such as diurnal variations [15].

Similar limitations are found in obtaining  $T_m$  parameters. Radiosonde profile data is the ideal way to get accurate  $T_m$ , which is unrealistic for GNSS stations due to high expenses [16]. Bevis proposed a  $T_m - T_s$  model as an alternative to retrieve  $T_m$  using surface in situ temperature [1]. The model works with dependence on the measured temperature data and the potential temporal variations from in situ  $T_s$  may introduce artificial signals in the retrieved PWV [17]. Additionally, the empirical models have been proposed to retrieve  $T_m$ , but they also have an insufficient accuracy in

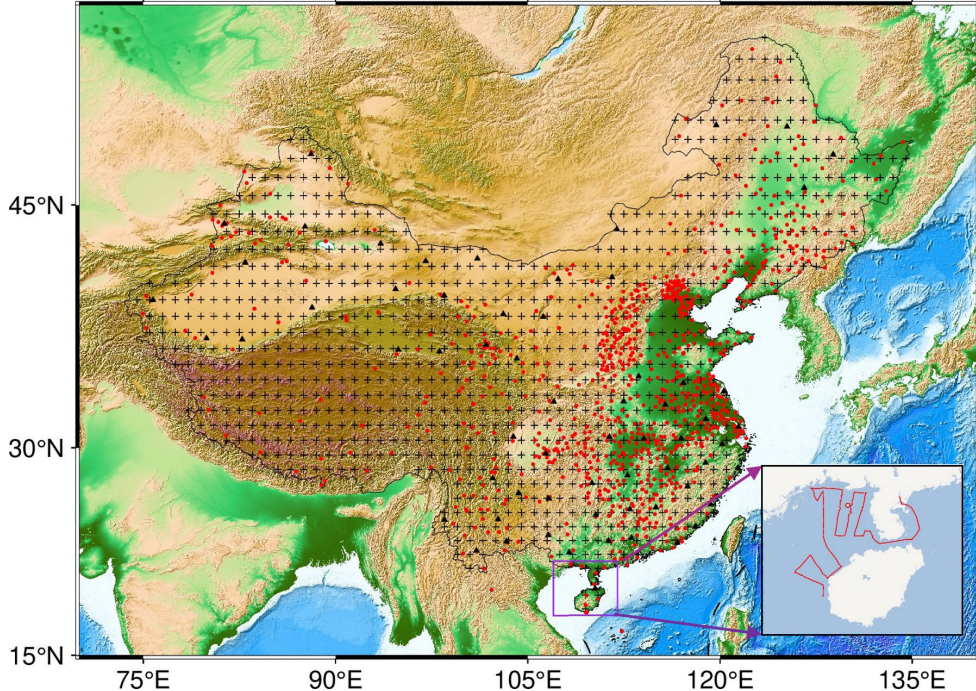


Fig. 1. Geographic distributions of the radiosonde (black triangle) and GNSS stations (red dots) and the grid points (blue cross) of the HDTM model; the voyage path (red line) over the South China Sea is presented as a subplot in a black box.

short-term variations, especially in severe weather conditions [18], [19], [20]. The machine learning (ML)-based models have been trained to directly retrieve PWV from ZTD [21], [22]. However, ML-based models are data-driven models with weak interpretability and their accuracy is limited in areas where data is distributed sparsely [23].

Numerical weather prediction (NWP) models have significant improvements in accuracy and spatial resolution and provide forecast tropospheric parameters [24], [25], [26], [27], such as the Global Forecast System (GFS) at the National Centers for Environmental Prediction (NCEP) and Integrated Forecasting System (IFS) at the European Centre for Medium-Range Weather Forecasts (ECMWF). It should be noted that IFS forecasts from ECMWF have recently been released to the public for free. The two models employ a grid-based system to simulate atmospheric processes and assimilate observation data, providing timely weather forecasts. However, NCEP-GFS and ECMWF-IFS differ in forecast step, time resolution, driving model, and assimilated observation data. These differences lead to variations in how each model incorporates observations and generates outputs [28], [29]. The two models are open for free and would be a reliable source of atmosphere research. Vienna University of Technology (TUW) utilizes the ECMWF forecasts to routinely produce a global ZHD grid for authorized users [10] but operates in a relatively coarse time resolution (6 h). This has a deficiency in PWV retrieval, especially in characterizing PWV short-term variation, when the weather changes rapidly [16], [30].

To improve time and accuracy, we proposed a novel model, called HDTM, which can provide hourly ZHD and T<sub>m</sub> grids, especially designed for real-time GNSS PWV retrieval, free from its dependency on in situ observations. The HDTM utilizes two freely available NWPs (NCEP-GFS

and ECMWF-IFS) to generate the ZHD and T<sub>m</sub> forecasts. To demonstrate the performance of HDTM in China, we evaluate the HDTM in three aspects: 1) overall accuracy; 2) performance in GNSS PWV retrieval; and 3) applicability in severe weather conditions.

The article is structured as follows. The used data are described in Section II and the methodology is presented in Section III. Evaluations and analysis of HDTM are presented in Section IV, along with two case studies covering extreme rainfall events. The conclusions are drawn in Section V.

## II. DATA DESCRIPTION

### A. GNSS and In Situ Meteorological Data

Two months of GNSS-ZTD and in situ pressure data at 953 GNSS stations over China were collected in 2023, with the ones observed in June representing the warm month and the ones in October representing the cold month. The ZHDs from in situ pressure are regarded as the basis for evaluating the accuracy of HDTM-ZHD. The GNSS stations cover an altitude range from sea level to almost 5000 m. In addition, we collected in situ pressure data using a shipborne barometer during a cruise campaign in the South China Sea and validated the performance of the HDTM model over the ocean. Ground-observed precipitation data are used to verify the performance of HDTM in extreme severe weather. Fig. 1 presents the geographic distribution of GNSS and radiosonde stations and the HDTM model grid points, along with the voyage path.

### B. Atmosphere Data

ERA5 is the fifth-generation reanalysis product of ECMWF and the successor of ERA-Interim [31]. The ERA5 products are released as hourly fields including geopotential height, air temperature, and specific humidity at 37 pressure levels

TABLE I  
CHARACTERISTICS OF DATA AND MODELS

Item	Time Interval	Horizontal resolution/ Stations number
HDTM(NCEP-GFS)	1 hour	$1^\circ \times 1^\circ$
HDTM(ECMWF-IFS)	3 hour	$1^\circ \times 1^\circ$
TUW	6 hour	$1^\circ \times 1^\circ$
ERA5	1 hour	$0.25^\circ \times 0.25^\circ$
Radiosonde	12 hour	64
GNSS-ZTD	30 min	953
Pressure	30 min	953
GNSS-PWV	30 min	953

from 1000 to 0.1 hPa, with a horizontal resolution of  $0.25^\circ$ . Furthermore, atmospheric profiles of 64 radiosondes were collected twice per day in 2023. They are obtained from the Department of Atmospheric Science of the University of Wyoming. For comparisons with the newly developed model, we make use of the ERA5 reanalysis data to calculate reference ZHDs. We integrate pressure level data from the top pressure level to grid point height with ERA5 profiles and calculate the ZHD above the top level with the Saastamoinen model. The sum of integral ZHD and modeled ZHD values is considered as ERA5-ZHD. We directly compare the difference between ERA5-ZHD and ZHD from HDTM among common epochs without any vertical correction. Besides, the RS- $T_m$  is calculated by the numerical integral of the radiosonde profiles at each station.

#### C. NWP Data

The new HDTM model is developed and released as a global grid at  $1^\circ \times 1^\circ$  horizontal resolution. ZHD and  $T_m$  at each grid point are integral results based on forecasts of NCEP-GFS and ECMWF-IFS and are provided 2–3 h in advance. NCEP-GFS and ECMWF-IFS are two typical NWP models, whose products are freely available for public use. It should be noted that open data in ECMWF-IFS have been improved from  $0.4^\circ$  to  $0.25^\circ$  in horizontal resolution and their forecasts have been provided for free since an IFS update in February 2024. We started providing IFS models on 16th March 2024 and HDTM(NCEP-GFS) and HDTM(ECMWF-IFS) are free for the public and are provided via an FTP server.

To avoid the impacts of interpolation errors, we only use data at common grid points directly at  $1^\circ \times 1^\circ$  resolution over China for the comparison to ERA5. Besides, TUW routinely produces a global ZHD grid as a by-product of Vienna mapping functions 3 (VMF3) using a ray-tracing technique. We use TUW as an additional external result to be compared. The characteristics of the datasets used in this article are summarized in Table I.

### III. METHODOLOGY

#### A. GNSS PWV Retrieval

The retrieval of PWV from GNSS ZTD is typically performed as follows: 1) first, separating ZWD from GNSS-ZTD by employing external ZHD and 2) second, converting the ZWD to PWV with the help of  $T_m$ . In the first step, ZHD is calculated from in situ pressure using the Saastamoinen

model or obtained from HDTM models [3]. In converting ZWD to PWV, the conversion factor  $\Pi$  can be obtained by  $T_m$  as follows [2]:

$$\text{PWV} = \Pi \cdot \text{ZWD} = \Pi \cdot (\text{ZTD} - \text{ZHD}) \quad (1)$$

$$\Pi = \frac{10^6}{\rho_w R_w \left( \frac{k_3}{T_m} + k'_2 \right)} \quad (2)$$

where  $\rho_w = 1 \times 10^3$  ( $\text{kg}/\text{m}^3$ ),  $k_3 = 3.739 \times 10^5$  ( $\text{K}^2/\text{hPa}$ ), and  $k'_2 = 16.52$  ( $\text{K}/\text{hPa}$ ) are refractivity constants [32];  $T_m$  is the weighted mean temperature (in K); and  $R_w = 461.495$  ( $\text{J} \cdot \text{K}^{-1} \cdot \text{kg}^{-1}$ ) is the gas constant for water vapor.

#### B. Establishment of the HDTM Model

ZHD and  $T_m$  are calculated by the numerical integral of the humidity, pressure, and temperature profiles from NCEP-GFS and ECMWF-IFS forecasts at each  $1^\circ \times 1^\circ$  grid point. The formula of ZHD calculation is presented as follows [4], [33]:

$$\text{ZHD} = 10^6 \sum_i^n \left[ \frac{(H_i - H_{i+1})(N_{H_i} - N_{H_{i+1}})}{\ln N_{H_i} - \ln N_{H_{i+1}}} \right] \quad (3)$$

$$N_h = k_1 R_d \left( \frac{e_d}{T \cdot R_d} - \frac{e_w}{T \cdot R_w} \right) \quad (4)$$

$T_m$  is defined as follows [34]:

$$T_m = \frac{\int_{H_g}^{\infty} \frac{e_w}{T} dh}{\int_{H_g}^{\infty} \frac{e_w}{T^2} dh} \quad (5)$$

where  $H_g$  (km) represents the grid point height;  $H_i$  (km) and  $N_{H_i}$  ( $\text{mm}/\text{km}$ ) are the height and dry air refractivity of the  $i$ th layer, respectively;  $e_d$  (hPa) and  $e_w$  (hPa) are the partial pressures for dry air and water vapor, which can be determined with pressure and specific humidity, respectively;  $T$  (K) is the temperature;  $k_1 = 77.6890$  ( $\text{K}/\text{hPa}$ ) is the refractivity constant;  $R_d = 287.053$  ( $\text{J} \cdot \text{K}^{-1} \cdot \text{kg}^{-1}$ ) is the gas constant for dry air.

#### C. Implementation of the HDTM Model

The vertical reduction of HDTM-ZHD follows three steps:

First, the ZHD at the grid point height ( $\text{ZHD}_g$ ) is converted to the respective pressure ( $P_g$ ) using

$$P_g = \text{ZHD}_g \cdot \frac{1 - 0.00266 \cdot \cos(2\varphi) - 0.00028 \cdot H_g}{0.0022793} \quad (6)$$

where  $\varphi$  (radians) is the grid point latitude and  $H_g$  (km) is the height of the grid point.

Then,  $P_g$  is adjusted from the grid height to the target height  $H_t$  using the improved vertical correction grid for pressure from the IGPZWD model [35]. The vertical accuracy and applicability of pressure are optimized by considering the annual and semi-annual harmonics for pressure height scale factors of exponential function with three orders. The coefficients at each grid point can be obtained according to respective longitude and latitude. The vertical correction reads as follows:

$$P_t = P_g \cdot \exp \left[ \sum_{n=1}^{n=3} \beta_n (H_t^n - H_g^n) \right] \quad (7)$$

where  $P_t$  is the pressure (hPa) at the target height and  $H_t$  is the target height (m).  $\beta_n$  denotes the vertical correction coefficients of  $n$ th order for pressure at the grid point.

Finally, the adjusted pressure is converted to ZHD again within the Saastamoinen model [3]. The implementation of such a tropospheric grid model requires a highly accurate vertical reduction function, which can adjust the tropospheric delay and  $T_m$  at the grid height to the site height.

As for the vertical reduction in  $T_m$ , we first introduce the formula from Askne and Nordius [2]

$$T_m = T_s \cdot \left(1 - \frac{\alpha R_d}{(\lambda + 1) g_m}\right) \quad (8)$$

$$T_t = T_s \cdot (P_t / P_s)^{\alpha R_d / g_m} \quad (9)$$

where  $T_s$  and  $T_t$  are the surface temperature (K) and the temperature (K) at the target height, respectively; and  $P_s$  and  $P_t$  denote the pressure at the surface and the target height, respectively. The former can be obtained with  $P_g$  in (6) and the latter is  $P_t$  in (7).  $\alpha$  denotes its temperature lapse rate (K/km);  $\lambda$  is the fit value for specific pressure; and  $g_m$  is mean gravity acceleration.

The vertical reduction method is derived from using (8) and (9) and we writes as follows:

$$\frac{T_m(H_t)}{T_m(H_g)} = \frac{T_s(H_t)}{T_s(H_g)} = \left(\frac{P_t}{P_g}\right)^{\alpha R_d / g_m} \quad (10)$$

where  $H_t$  and  $H_g$  denote the target height and grid point height, respectively;  $T_m(H_t)$  and  $T_m(H_g)$  are  $T_m$  at the target height and grid point height, respectively; and  $P_t$  and  $P_g$  are the pressure at the target height and grid point height, respectively. After applying the height adjustment, we use the bilinear interpolation method to obtain ZHD and  $T_m$  at the site position.

#### IV. RESULTS

In this section, we use multisource ZHD and  $T_m$  to validate HDTM over land and ocean, including ERA5, radiosonde profiles, and pressure-derived ZHD. Next, we utilize the HDTM model in GNSS-PWV retrieval and assess the performance of HDTM-based PWV retrieval over China using the PWV based on meteorological observations. Finally, we present two extreme precipitation events to demonstrate the performance of HDTM in retrieving GNSS-PWVs.

##### A. Validation of HDTM-ZHD

1) *HDTM-ZHD Over Land and Ocean*: To show the overall performance of HDTM-ZHD over China, Table II presents the biases and standard deviations (STDs) of three ZHD products, including HDTM(NCEP-GFS), HDTM(ECMWF-IFS), and TUW model. The ERA5 is used as a reference. The data period covers 45 days from 16 March to 30 April 2024. Both HDTM models show accurate ZHD with root mean square (rms) errors of below 2.7 mm. HDTM(NCEP-GFS)-ZHD shows mean biases of  $-1.4$  mm and mean STD of 1.5 mm, while HDTM(ECMWF-IFS) shows mean biases of  $-2.2$  mm and mean STD of 1.6 mm. In comparison, TUW

TABLE II  
BIASES AND STD OF ZHD FROM THREE MODELS WITH RESPECT TO ERA5

Item	Biases (mm)	STD (mm) Mean [Min/Max]	RMS (mm)
			2.1 [1.2/4.2]
HDTM (NCEP-GFS)	-1.4 [-3.9/1.1]	1.5 [1.0/2.8]	2.1 [1.2/4.2]
HDTM (ECMWF-IFS)	-2.2 [-4.1/-0.5]	1.6 [0.9/2.3]	2.7 [1.5/4.5]
TUW(FC) (interpolated)	-0.7 [-2.9/1.9]	2.1 [0.9/9.4]	2.3 [1.0/9.4]

provides hourly interpolated ZHD with an rms of 2.3 mm but reaches a maximum STD of 9.4 mm in the worst case.

Furthermore, the spatial distribution of biases and STD of ZHD from HDTM(NCEP-GFS) and HDTM(ECMWF-IFS) over China is also shown in Fig. 2. HDTM(ECMWF-IFS)-based results show a larger bias over China than HDTM(NCEP-GFS) ones. The reason for the slightly worse performance of HDTM(ECMWF-IFS) could be because the number of pressure layers of ECMWF-IFS is less than the layer numbers of the NCEP-GFS model. Both models also show that the larger STD appears in the Hengduan Mountains and Sichuan Basin, reaching an STD of 2.3 mm.

To validate the performance of HDTM-ZHD over land, we compare the HDTM-ZHD to the pressure-derived ZHD from 953 GNSS/MET sites in Fig. 3. Considering that similar performances are obtained by those two HDTM models, only HDTM(NCEP-GFS) is used to demonstrate the HDTM performance because ECMWF-IFS is not available during this period. Differing from the comparison with ERA5, the site ZHD needs to be vertically corrected and horizontally interpolated, which causes an accuracy reduction. However, the results of 953 stations indicate that HDTM can provide an accurate site ZHD with a mean rms of 3.2 mm, in general, including a mean bias of  $-1.5$  mm and a mean STD of 2.1 mm. As for the regional difference in ZHD errors, there is a negative bias in ZHD from HDTM(NCEP-GFS) over the Hengduan Mountains. Moreover, the rms is slightly larger than in other areas, which is also confirmed by the comparison with ERA5.

To demonstrate the HDTM performance over the ocean, we compare the ZHD from HDTM(NCEP-GFS) with in situ pressure data as shown in Fig. 4. As an existing model, the results from the TUW model are also plotted. The HDTM(NCEP-GFS) model achieved 1.9 mm in rms while the TUW model showed an rms of 3.4 mm, demonstrating superior performance compared to the TUW model. The HDTM-ZHD has improved around 44% in mean rms over the ZHD from the TUW model. The finding indicates that the HDTM model performs better than the TUW model in providing ZHD and would be a potential approach to achieve oceanic PWV monitoring.

Overall, the in situ pressure results confirm that the HDTM model provides ZHD with mean rms errors of 3.2 mm over land and 1.9 mm for oceanic scenarios. When compared with ERA5, the HDTM shows 2.1 mm in rms and presents better ZHD forecasts over TUW models.

2) *Advantages in Diurnal Variation*: To investigate the temporal advantages of HDTM-ZHD in diurnal variation, Fig. 5

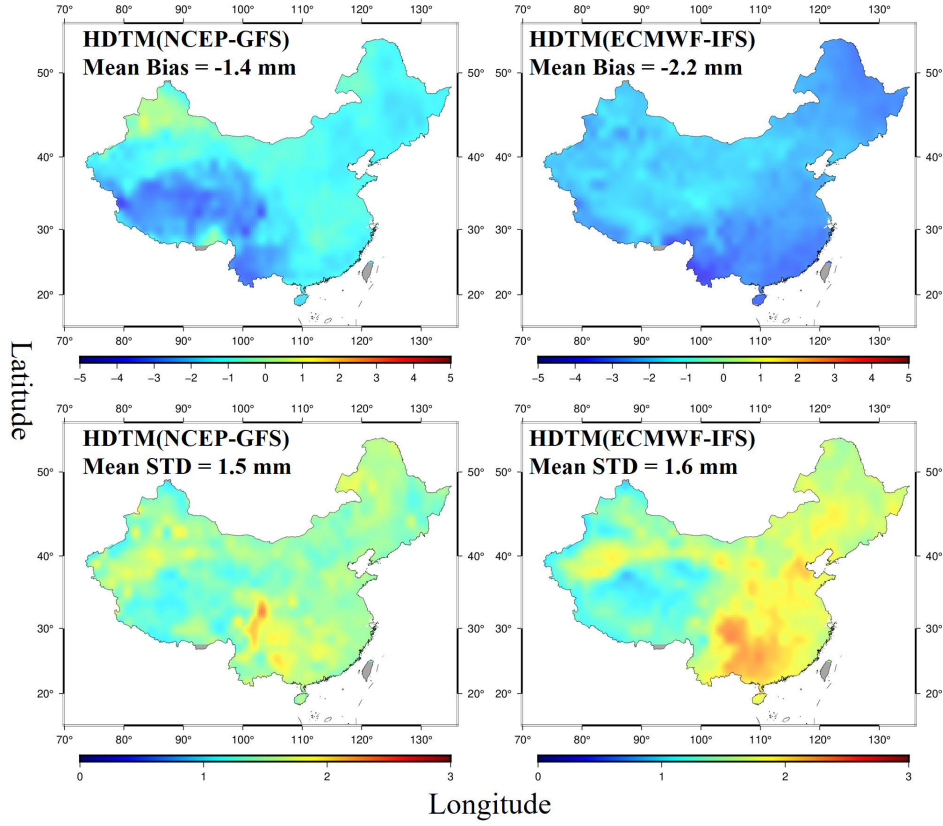


Fig. 2. Biases (mm) and STD (mm) errors of (left) HDTM(NCEP-GFS)-ZHDs and (right) HDTM(ECMWF-IFS)-ZHDs with respect to the ERA5-derived ZHDs.

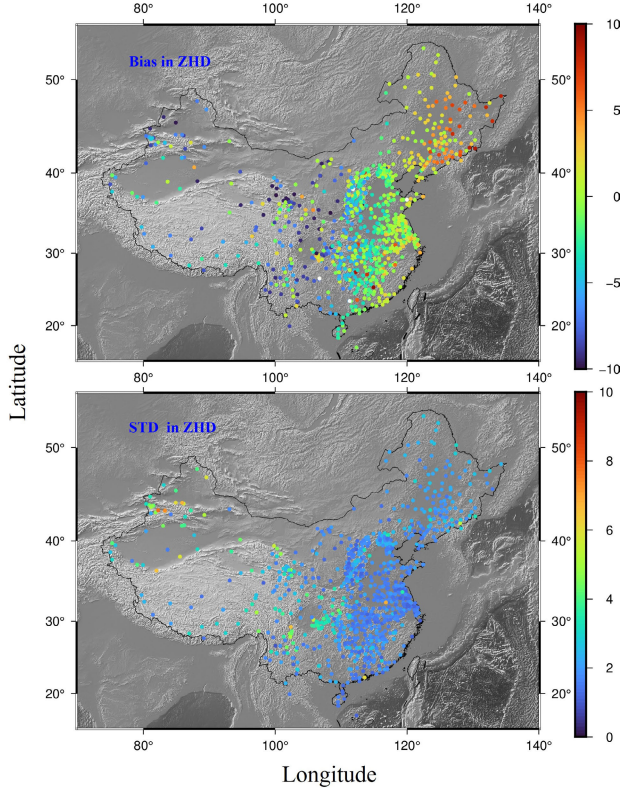


Fig. 3. (Top) Biases (mm) and (bottom) STD (mm) errors of HDTM ZHD with respect to the in situ pressures derived ZHD.

presents three approaches for providing ZHD at JSYZ, BGNW, and BFTO stations, including HDTM(NCEP-GFS), TUW, and

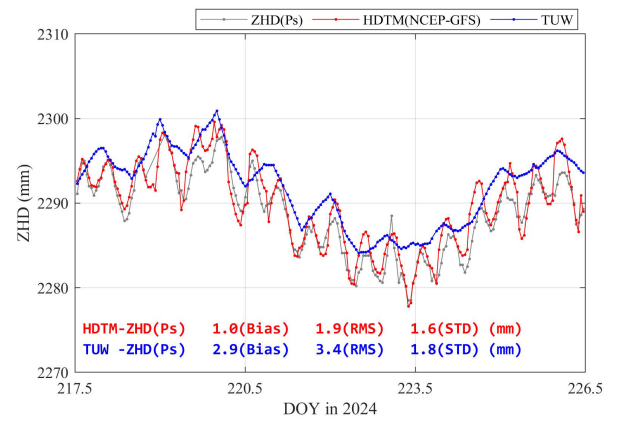


Fig. 4. Time series of ZHD (mm) obtained from HDTM(NCEP-GFS) and TUW over ocean. The ZHD from the shipborne barometer is also presented as references.

GPT3 models, with in situ pressure-derived ZHD provided as a reference. To make our result representative, we selected three typical stations from different climate zones and elevations. The HDTM provides hourly ZHD while the TUW provides ZHD with 6-h intervals. TUW-ZHD can be interpolated into the 1-h, which has an accuracy reduction. We found a consistency of less than 2 mm in rms between HDTM-ZHD and the pressure-derived ZHD during diurnal variations. TUW-ZHD performs worse than the HDTM(NCEP-GFS) model, which exhibited significant fitting errors and larger rms values at the interpreted epoch, indicating that the 6-h temporal resolution of the TUW models is insufficient for capturing

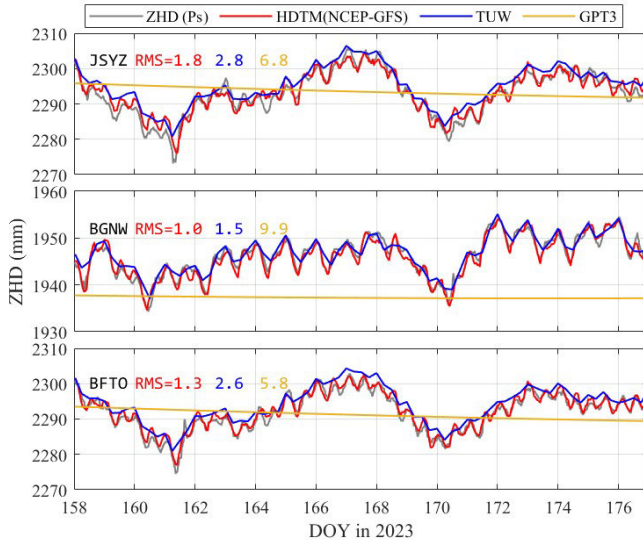


Fig. 5. Time series of ZHD (mm) obtained from HDTM(NCEP-GFS), TUW, and GPT3 models at JSYZ, BGNW and BFTO stations. The ZHD from in situ pressure is also presented as references.

hourly variations in ZHD. The GPT3 empirical model shows the largest rms, indicating it falls at the diurnal scale.

To show the performance of HDTM on the diurnal cycle, the mean biases at different hours of the day at three stations are presented in Fig. 6. Since GPT3 performs worse on the diurnal scale as shown in Fig. 5, we only compare the results from TUW and HDTM(NCEP-GFS). The hourly ZHD from HDTM(NCEP-GFS) shows superior accuracy and stability, as seen at the BGNW station. The STD of the TUW-ZHD exhibits a pronounced periodic effect on the diurnal cycle due to interpolation, which is particularly noticeable at the BFTO station. The biases of hourly ZHD from the TUW model are twice as large as those from HDTM(NCEP-GFS).

Therefore, we confirm that HDTM can provide improved real-time ZHD on the diurnal cycle when compared to the TUW model and GPT3 model due to its high temporal resolution and accurate forecasts, showing the advantages of capturing more detailed variation of ZHD.

#### B. Evaluation of HDTM- $T_m$

1) *Overall Performance of HDTM- $T_m$ :* To demonstrate the performance of HDTM- $T_m$  over China, as shown in Fig. 7, we compared  $T_m$  from HDTM(NCEP-GFS) and HDTM(ECMWF-IFS) with ERA5- $T_m$ . HDTM(NCEP-GFS) can provide  $T_m$  with biases of  $-0.1$  K and STD of  $1.1$  K while HDTM(ECMWF-IFS) can provide  $T_m$  with biases of  $-0.7$  K and STD of  $1.0$  K. As for the geographical distribution of  $T_m$  errors, Fig. 7 shows that biases of HDTM- $T_m$  are slightly worse on the Tibetan plateau (TP) and surrounding areas, which is related to the complex terrain. Nevertheless, the results over other areas show a good performance with biases of below  $0.5$  K. It is noted that an uncertainty of  $5$  K in  $T_m$  corresponds to  $1.7\%-2.0\%$  in PWV [36]. Considering this fact, both HDTM(NCEP-GFS) and HDTM(ECMWF-IFS) can provide high-quality  $T_m$  to support real-time PWV retrieval, which is a lack of current traditional methods and models.

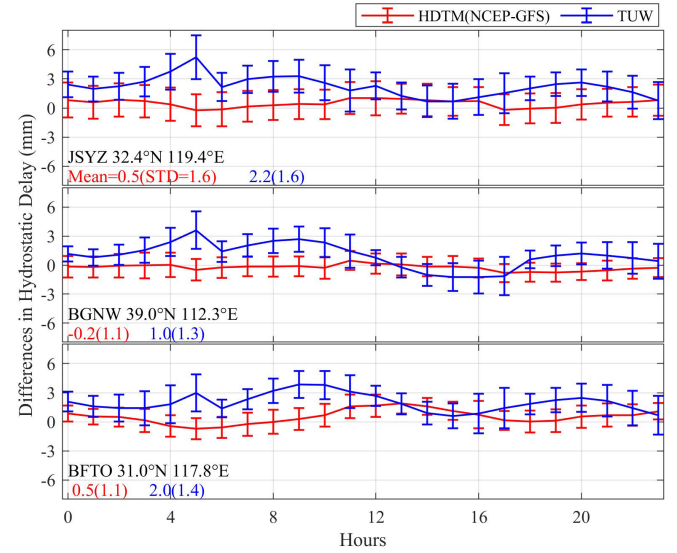


Fig. 6. Biases variation (mm) of the hourly ZHD diurnal cycle from HDTM and TUW at JSYZ, BGNW, and BFTO stations. The ZHD from measured situ pressure is also presented as a reference.

TABLE III  
BIASES (K) AND STD (K) OF  $T_m$  FROM HDTM AND BEVIS METHOD  
AT 64 RADIOSONDE STATIONS WITH RESPECT TO RADIOSONDE  
PROFILE RESULTS

Item	Biases (K)	STD (K)	RMS (K)
		Mean [Min/Max]	
HDTM (NCEP-GFS)	-0.2 [-1.8/1.8]	1.4 [0.8/2.2]	1.5 [0.8/2.5]
Bevis	-0.4 [-2.9/4.4]	2.3 [1.5/2.9]	2.5 [2.0/3.0]

To further validate the implementation performance in real cases, biases and STD geographical distributions of  $T_m$  from HDTM and Bevis method with respect to RS- $T_m$  at 64 radiosonde sites are presented in Fig. 8. Radiosonde profiles record the in situ atmospheric status at pressure levels, which provide more accurate references for  $T_m$  than ERA5. Bevis- $T_m$  are calculated by the Bevis model using the in situ temperature of the lowest layer of the radiosonde profile for comparison [1]. HDTM(NCEP-GFS)- $T_m$  shows a mean rms of  $1.5$  K, reaching an average bias of  $-0.2$  K and an STD of  $1.4$  K with respect to RS- $T_m$ , which indicates an improvement compared to the Bevis model. The statistical results in  $T_m$  of all 64 radiosondes in Table III show that HDTM- $T_m$  performs better in bias and STD, reducing around  $40\%$  in mean rms compared to the Bevis method.

The comparison results confirm that HDTM can provide a high quality of  $T_m$  forecast with an rms of around  $1.5$  K, showing comparable quality with ERA5 reanalysis and radiosondes. This is also the first release of  $T_m$  at a horizontal resolution of  $1^\circ$  as gridded forecasts products.

2) *Advantages in Diurnal Variation:* To show the advantages in temporal resolution of HDTM- $T_m$ , we use the four approaches to calculate  $T_m$  at NMEL and JLLJ stations from different climate zones in Fig. 9, including HDTM(NCEP-GFS), ERA5, GPT3, and the Bevis model. The rms of HDTM(NCEP-GFS)- $T_m$  reduces over  $3$  K in both stations when compared with GPT3. This is related to the diurnal

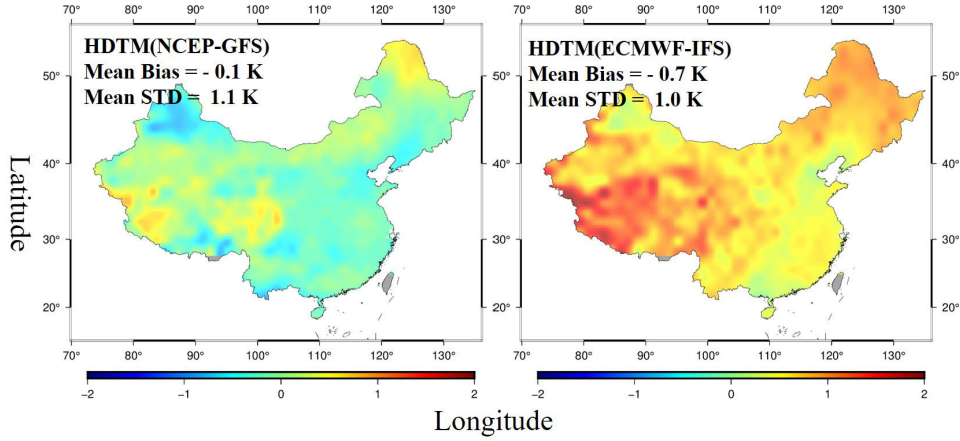


Fig. 7. Biases (K) of  $T_m$  from HDTM(NCEP-GFS) and HDTM(ECMWF-IFS) with respect to ERA5.

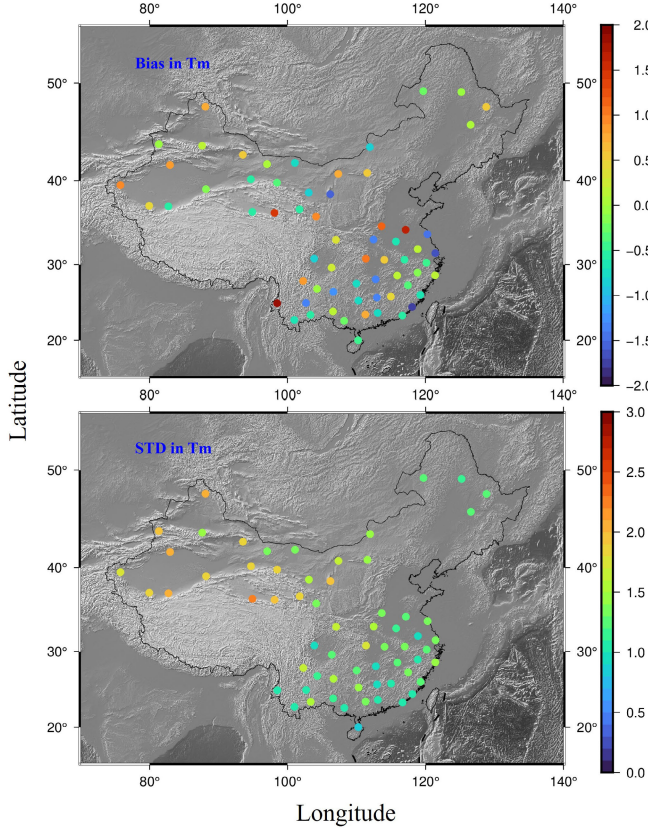


Fig. 8. (Top) Biases (K) and (bottom) STD (K) errors of HDTM- $T_m$  w.r.t RS- $T_m$  at 64 radiosonde stations.

variations, which are not captured in GPT3. The Bevis- $T_m$  performs better than GPT3- $T_m$ , but it absorbs the diurnal variation from surface temperature, showing a periodic shift. It should be noted that Bevis- $T_m$  relies on the measured surface temperature and its accuracy does not have equivalent performance over all stations.

However, HDTM- $T_m$  has an rms of around 1 K and is provided with hourly updates, showing a significant improvement compared to the GPT3 and Bevis models. Besides, HDTM- $T_m$  is driven by NWP forecasts and has equivalent accuracy

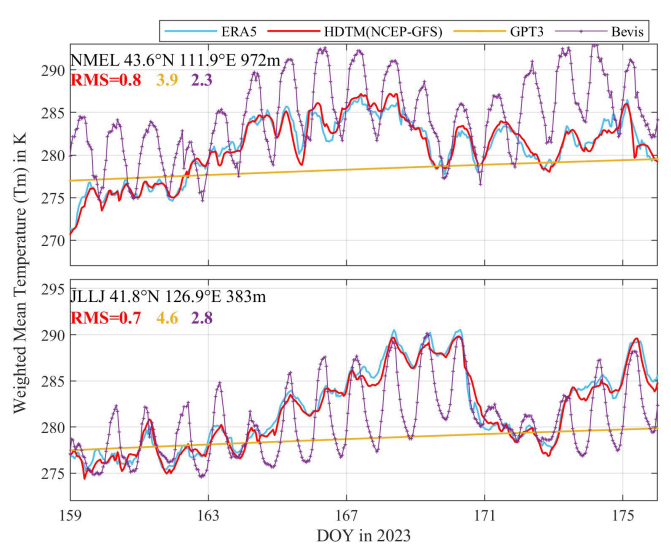


Fig. 9. Time series of  $T_m$  (in K) obtained from ERA5, HDTM(NCEP-GFS), GPT3, and Bevis models at NMEL and JLLJ station. The rms of  $T_m$  of different methods relative to ERA5 are listed.

performance over China. Thus, it is obvious that HDTM- $T_m$  has a better performance in terms of accuracy consistency and would reduce the error from  $T_m$  for PWV retrieval.

### C. Overall Quality of HDTM-Based GNSS PWV

We present the overall performance of GNSS-PWV based on HDTM(NCEP-GFS) models, namely GNSS-PWV(HDTM), using PWV retrieved from postprocessing GNSS ZTD and in situ meteorological parameters as a reference (hereafter referred to as RF-PWV). The site ZHD is calculated with in situ pressure, and the  $T_m$  is calculated from the Bevis formula with in situ temperature as input.

To show the performance of HDTM-based GNSS-PWV retrieval over China, the spatial distribution of biases and STD of PWV (mm) at 953 GNSS sites are presented in Fig. 10. The statistical results in PWV of 953 GNSS/Met stations are presented in Table IV. As for geographical distribution, the HDTM model achieves better results in eastern China while

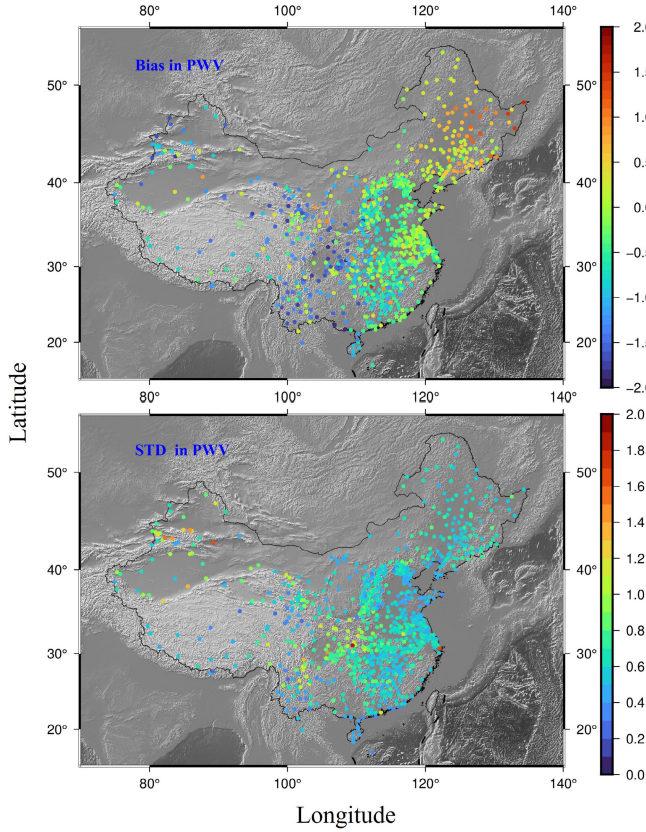


Fig. 10. Biases (mm) and STD (mm) of GNSS PWV results based on HDTM grid products. Using GNSS-PWV with in situ meteorological data as a reference.

TABLE IV  
BIASES AND STD OF GNSS PWV RESULTS BASED ON  
HDTM(NCEP-GFS) COMPARED TO RF-PWV

Item	Biases (mm)	STD (mm)	RMS (mm)
Mean	-0.5	0.6	0.9
Min	-1.9	0.2	0.3
Max	1.6	1.8	2.1

they mainly exhibit positive bias in the northeastern region. The results at the edge of the TP and the Hengduan Mountains are worse, as some stations show biases of over 1.5 mm. GNSS-PWV(HDTM) is prone to ZHD and  $T_m$  vertical correction errors caused by high height differences [30]. Overall, the results demonstrate that HDTM-based GNSS-PWV with a mean rms of 0.9 mm shows satisfactory performance over China, reaching mean biases of  $-0.5$  mm and STD of 0.6 mm in PWV differences at 953 stations with respect to the PWV results with in situ meteorological data.

The results show that HDTM can work for real-time water vapor retrieval and only introduce rms of about 1 mm in PWV differences with respect to the conventional method, which relies on the in situ meteorological data. Thus, HDTM can be conveniently used in aiding real-time GNSS-PWV retrieval at hourly rates for existing monitoring networks without any extra meteorological devices.

#### D. HDTM-Based GNSS PWV in Severe Weather

To validate the performance of HDTM in GNSS PWV retrieval under turbulent weather conditions, we analyzed two

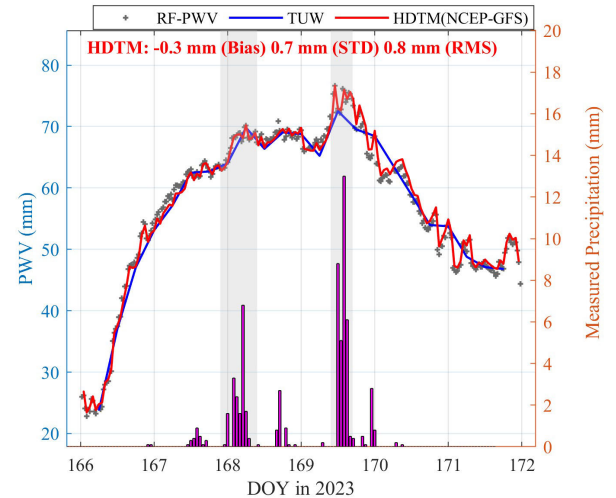


Fig. 11. Time series of RF-PWV (gray), GNSS-PWV(HDTM) (red), and GNSS-PWV(TUW) (blue) and measured precipitation (magenta) (mm) at the BTCD station under extreme heavy rainfall conditions.

significant heavy rainfall events: one in Wuhan in June 2023, and another during Typhoon “Sanba” in October 2023. Using GNSS-PWV retrieved with in situ meteorological parameters as a reference (RF-PWV), we assessed the performance of the HDTM-based GNSS-PWV (referred to as GNSS-PWV (HDTM)) under extreme weather conditions. We also present results using the TUW model for comparison purposes.

1) *Case A (Heavy Rainfall in Wuhan):* As shown in Fig. 11, Wuhan experienced two major precipitation events, with the second being more intense. The main precipitation periods are masked as gray. Before the rainfall, a significant and rapid increase in PWV was detected by GNSS-PWV(HDTM). During the second rainfall, GNSS-PWV(HDTM) exhibited strong consistency with RF-PWV, particularly capturing the brief decrease and subsequent rebound in water vapor during the event. This closely matches the recorded precipitation data, where rainfall decreased after the initial peak and then rose again. As for the TUW-based result, it fails to detect variations at PWV peak during the event during DOY 169–170 but records the peak PWV successfully in DOY 168. Compared to the rainfall in DOY 168, the latter rainfall is more intense and the ZHD exhibits significant short-term variation. The failure in capturing peak PWV is related to the joint effect of the intensity of the precipitation and the sparser temporal resolution of TUW-based results.

Even in heavy rainfall conditions, the HDTM-based PWV retrieval maintained high-precision hourly water vapor monitoring, with a PWV bias of only 0.3 mm. In contrast, the GNSS-PWV(TUW) with 6-h intervals underestimated the PWV peak and failed to detect variations in PWV during the event.

After the rainfall event, PWV showed a clear downward trend, signaling the end or pause of precipitation. The actual RF-PWV (30-min intervals) indicated that the PWV descent occurred in a “stepwise” fashion, with brief increases during the decline. GNSS-PWV(HDTM) successfully characterized this detailed process. However, GNSS-PWV(TUW) displayed

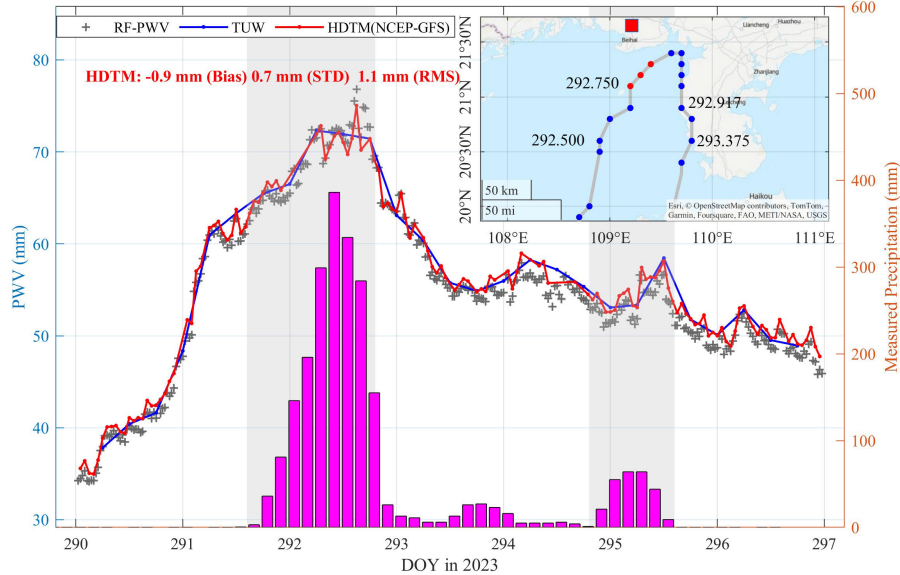


Fig. 12. Time series of RF-PWV (gray), GNSS-PWV(HDTM) (red), and GNSS-PWV(TUW) (blue) (mm) and measured precipitation (magenta) (mm) at GXBH station during typhoon “Sanba.” The typhoon path on DOY 292–293 is plotted in the subplot. The red circle points in the typhoon track subplot refer to the STS track while the blue points refer to the tropical storm track. The red rectangle represents the GXBH GNSS site. The numbers near track points are the time in DOY of the Typhoon Center at this location.

a constant descent rate, only roughly reflecting the PWV trend due to its limited temporal resolution. The result indicates that the 6-h interval PWV is insufficient to capture the rapid changes in water vapor, which is crucial for short-term weather forecasting.

2) *Case B (Typhoon “Sanba”):* To evaluate the HDTM applicability in Typhoon events, we also analyzed the HDTM(NCEP-GFS)-based PWV results during typhoon “Sanba” in Fig. 12. The GXBH station is located within the influence radius of the severe tropical storm, which experienced severe rainfall during this period. Taking advantage of higher temporal resolution, GNSS-PWV(HDTM) effectively captures the process of water vapor increase. At the peak of precipitation, the change in water vapor was detected, and the continuous decline in PWV was observed earlier (along the right edge of the first heavy rainfall shadow), providing early signals of the event’s end or pause. However, PWV results with 6-h intervals often failed to quickly and accurately capture the timing of precipitation events. Overall, the HDTM model provided high-resolution (1-h interval) PWV results in real time with an rms of 1.1 mm compared to the conventional approach during typhoons and heavy rainfall events (up to 128 mm/h). This also demonstrates the HDTM model’s capability to forecast ZHD and  $T_m$  in severe weather conditions accurately.

In conclusion, the HDTM-based approach effectively reflects the temporal variation of water vapor in real time under extreme weather conditions. This capability potentially supports fast and accurate real-time GNSS-PWV retrievals in extreme weather.

## V. CONCLUSION

This work introduces the HDTM model, which has significantly advanced in providing timely ZHD and weighted mean

temperature for real-time GNSS-PWV retrieval. Two advanced NWP models, NCEP GFS and ECMWF IFS (newly free to the public), are utilized in developing the HDTM model. Compared with the original NWP data, the HDTM model compressed high-volume data into a horizontal grid of a single level with accurate modeling of highly variable ZHD and  $T_m$ . The HDTM model was evaluated based on three aspects: parameter accuracy, practicality in GNSS-PWV retrieval, and performance in severe weather conditions, demonstrating substantial improvements in several key areas.

- 1) *Performance and Advantages in ZHD and  $T_m$ :* The HDTM model can provide hourly ZHD forecasts with a mean rms of 3.2 mm for land and 1.9 mm for the ocean se, respectively. Compared with the TUW-ZHD, the HDTM provides higher time resolution and performs better in diurnal scales, reducing 44% in the rms of oceanic ZHD. High-quality HDTM- $T_m$  with a mean rms of below 1.5 K are verified by ERA5 and radiosondes, and perform in diurnal variation, showing around 40% reduction in mean rms compared to the Bevis method. It is concluded that HDTM outperforms the traditional method in parameter quality, diurnal variation, and time resolution.
- 2) *Accurate PWV Retrieval:* We used the HDTM model for real-time GNSS PWV retrieval at 953 sites in China. The results show the HDTM model only introduces the error with a mean rms of 0.9 mm in retrieved PWV with respect to in situ meteorological parameters. This demonstrates that the HDTM approach effectively circumvents reliance on in situ parameters, streamlining real-time PWV retrieval. We implemented HDTM to retrieve real-time GNSS PWV at 953 GNSS/MET sites over China and achieved a comparable result with the in situ parameters-derived PWV with mean rms of

0.9 mm, introducing mean biases of  $-0.5$  mm and mean STD of 0.6 mm in PWV differences. This demonstrates that the HDTM approach effectively circumvents reliance on in situ parameters, streamlining real-time PWV retrieval.

- 3) *Adaptability in Extreme Weather Conditions:* We showcased the model's capability in two severe rainfall events, illustrating its effectiveness in capturing small-scale variations and trends in PWV before, during, and after such events. TUW fails in detecting the PWV peaks due to the joint effect of sparse ZHDs and highly variable ZHDs in severe precipitation. This adaptability positions HDTM as a promising model for real-time GNSS-PWV retrieval, offering more timely and accurate water vapor monitoring than traditional methods.

In conclusion, the HDTM model not only surpasses conventional models in accuracy and practicality but also paves the way for innovative approaches to real-time GNSS-PWV retrieval, particularly in challenging weather conditions. By breaking free from reliance on in situ meteorological data, HDTM represents a crucial step forward in the field. Future work should focus on refining the model's performance in complex terrains and exploring its application in extreme weather monitoring.

#### ACKNOWLEDGMENT

The authors would like to thank the China Meteorological Administration (CMA), TUW, ECMWF, NCEP, and the University of Wyoming for furnishing the relevant data.

#### REFERENCES

- [1] M. Bevis, S. Businger, T. A. Herring, C. Rocken, R. A. Anthes, and R. H. Ware, "GPS meteorology: Remote sensing of atmospheric water vapor using the global positioning system," *J. Geophys. Res.*, vol. 97, no. D14, pp. 15787–15801, Oct. 1992.
- [2] J. Askne and H. Nordius, "Estimation of tropospheric delay for microwaves from surface weather data," *Radio Sci.*, vol. 22, no. 3, pp. 379–386, May 1987.
- [3] J. Saastamoinen, "Atmospheric correction for the troposphere and stratosphere in radio ranging satellites," *Use Artif. Satell. Geodesy*, vol. 15, pp. 247–251, Jan. 1972.
- [4] B. Chen, W. Yu, W. Wang, Z. Zhang, and W. Dai, "A global assessment of precipitable water vapor derived from GNSS zenith tropospheric delays with ERA5, NCEP FNL, and NCEP GFS products," *Earth Space Sci.*, vol. 8, no. 8, pp. 1–22, Aug. 2021.
- [5] S. Jade and M. S. M. Vijayan, "GPS-based atmospheric precipitable water vapor estimation using meteorological parameters interpolated from NCEP global reanalysis data," *J. Geophys. Res., Atmos.*, vol. 113, no. D3, pp. 1–12, Feb. 2008.
- [6] D. Landskron and J. Böhm, "VMF3/GPT3: Refined discrete and empirical troposphere mapping functions," *J. Geodesy*, vol. 92, no. 4, pp. 349–360, Apr. 2018.
- [7] L. Huang et al., "Evaluation of hourly PWV products derived from ERA5 and MERRA-2 over the Tibetan plateau using ground-based GNSS observations by two enhanced models," *Earth Space Sci.*, vol. 8, no. 5, pp. 1–22, May 2021.
- [8] L. Huang et al., "GNSS precipitable water vapor retrieval with the aid of NWM data for China," *Earth Space Sci.*, vol. 8, no. 9, pp. 1–18, Sep. 2021.
- [9] K. Quinn and T. Herring, "GPS atmospheric water vapor measurements without the use of local barometers," *Eos Trans. AGU*, vol. 77, no. 46, p. 1996, 1996.
- [10] J. Böhm, R. Heinzelmann, and H. Schuh, "Short Note: A global model of pressure and temperature for geodetic applications," *J. Geodesy*, vol. 81, no. 10, pp. 679–683, Oct. 2007.
- [11] K. Lagler, M. Schindelegger, J. Böhm, H. Krásná, and T. Nilsson, "GPT2: Empirical slant delay model for radio space geodetic techniques," *Geophys. Res. Lett.*, vol. 40, no. 6, pp. 1069–1073, Mar. 2013.
- [12] J. Böhm, G. Möller, M. Schindelegger, G. Pain, and R. Weber, "Development of an improved empirical model for slant delays in the troposphere (GPT2w)," *GPS Solutions*, vol. 19, no. 3, pp. 433–441, Jul. 2015.
- [13] Y. Yao, C. He, B. Zhang, and C. Xu, "A new global zenith tropospheric delay model GZTD," *Chin. J. Geophys.*, vol. 56, no. 7, pp. 2218–2227, Jan. 2013.
- [14] Y. Yao, Y. Hu, C. Yu, B. Zhang, and J. Guo, "An improved global zenith tropospheric delay model GZTD2 considering diurnal variations," *Nonlinear Processes Geophys.*, vol. 23, no. 3, pp. 127–136, May 2016.
- [15] T. Li et al., "Refining the empirical global pressure and temperature model with the ERA5 reanalysis and radiosonde data," *J. Geodesy*, vol. 95, no. 3, pp. 1–17, Mar. 2021.
- [16] W. Zhang et al., "On the suitability of ERA5 in hourly GPS precipitable water vapor retrieval over China," *J. Geodesy*, vol. 93, no. 10, pp. 1897–1909, Oct. 2019.
- [17] W. Zhang, Y. Lou, J. Huang, and W. Liu, "A refined regional empirical pressure and temperature model over China," *Adv. Space Res.*, vol. 62, no. 5, pp. 1065–1074, Sep. 2018.
- [18] R. F. Leandro, R. B. Langley, and M. C. Santos, "UNB3m\_pack: A neutral atmosphere delay package for radiometric space techniques," *GPS Solutions*, vol. 12, no. 1, pp. 65–70, Jan. 2008.
- [19] Y. Yao, B. Zhang, C. Xu, and F. Yan, "Improved one/multi-parameter models that consider seasonal and geographic variations for estimating weighted mean temperature in ground-based GPS meteorology," *J. Geodesy*, vol. 88, no. 3, pp. 273–282, Mar. 2014.
- [20] Y. Yao, S. Zhu, and S. Yue, "A globally applicable, season-specific model for estimating the weighted mean temperature of the atmosphere," *J. Geodesy*, vol. 86, no. 12, pp. 1125–1135, Dec. 2012.
- [21] X. Zhao, Q. Niu, Q. Chi, J. Chen, and C. Liu, "A new LSTM-based model to determine the atmospheric weighted mean temperature in GNSS PWV retrieval," *GPS Solutions*, vol. 28, no. 2, p. 74, Apr. 2024.
- [22] Y. Zheng, C. Lu, Z. Wu, J. Liao, Y. Zhang, and Q. Wang, "Machine learning-based model for real-time GNSS precipitable water vapor sensing," *Geophys. Res. Lett.*, vol. 49, no. 3, pp. 1–10, Feb. 2022.
- [23] L. Huang, D. Lu, F. Chen, H. Zhang, G. Zhu, and L. Liu, "A deep learning-based approach for directly retrieving GNSS precipitable water vapor and its application in typhoon monitoring," *IEEE Trans. Geosci. Remote Sens.*, vol. 62, 2024, Art. no. 4111712.
- [24] C. Lu et al., "Improving BeiDou real-time precise point positioning with numerical weather models," *J. Geodesy*, vol. 91, no. 9, pp. 1019–1029, Sep. 2017.
- [25] C. Lu et al., "Tropospheric delay parameters from numerical weather models for multi-GNSS precise positioning," *Atmos. Meas. Techn.*, vol. 9, no. 12, pp. 5965–5973, Dec. 2016.
- [26] J. G. Powers et al., "The weather research and forecasting model: Overview, system efforts, and future directions," *Bull. Amer. Meteorolog. Soc.*, vol. 98, no. 8, pp. 1717–1737, Aug. 2017.
- [27] Z. Wu et al., "Evaluation of shipborne GNSS precipitable water vapor over global oceans from 2014 to 2018," *IEEE Trans. Geosci. Remote Sens.*, vol. 60, 2022, Art. no. 5802515.
- [28] L. Bengtsson and J. Han, "Updates to NOAA's unified forecast system's cumulus convection parameterization scheme between GFSv16 and GFSv17," *Weather Forecasting*, vol. 39, no. 11, pp. 1559–1570, Nov. 2024.
- [29] A. Persson and F. Grazzini, "User guide to ECMWF forecast products," *Meteorological Bull.*, vol. 3, no. 2, 2007.
- [30] H. Zhang, Y. Yuan, W. Li, D. Ji, and M. Lv, "Implementation of ready-made hydrostatic delay products for timely GPS precipitable water vapor retrieval over complex topography: A case study in the Tibetan plateau," *IEEE J. Sel. Topics Appl. Earth Observ. Remote Sens.*, vol. 14, pp. 9462–9474, 2021.
- [31] H. Hersbach et al., "The ERA5 global reanalysis," *Quart. J. Roy. Meteorol. Soc.*, vol. 146, no. 730, pp. 1999–2049, Jul. 2020.
- [32] J. M. Rüeger, "Refractive index formulae for radio waves," in *Proc. FIG 22nd Int. Congr.*, vol. 113, Washington, DC, USA, Jan. 2002, pp. 1–13.
- [33] B. Chen and Z. Liu, "A comprehensive evaluation and analysis of the performance of multiple tropospheric models in China region," *IEEE Trans. Geosci. Remote Sens.*, vol. 54, no. 2, pp. 663–678, Feb. 2016.

- [34] J. L. Davis, T. A. Herring, I. I. Shapiro, A. E. E. Rogers, and G. Elgered, "Geodesy by radio interferometry: Effects of atmospheric modeling errors on estimates of baseline length," *Radio Sci.*, vol. 20, no. 6, pp. 1593–1607, Nov. 1985.
- [35] C. Jiang et al., "An improved global pressure and ZWD model with optimized vertical correction considering the spatial-temporal variability of multiple height scale factors," *EGUsphere*, vol. 2024, pp. 1–25, Jan. 2024.
- [36] S. Hagemann, L. Bengtsson, and G. Gendt, "On the determination of atmospheric water vapor from GPS measurements," *J. Geophys. Res., Atmos.*, vol. 108, no. D21, p. 4678, Nov. 2003.



**Luohong Li** is currently pursuing the Ph.D. degree with the Innovation Academy for Precision Measurement Science and Technology (APM), Chinese Academy of Sciences (CAS), Wuhan, China.

He is working as a Visiting Ph.D. Student with the Space Geodesy Group, ETH Zürich, Zürich, Switzerland. His research focuses on GNSS atmosphere monitoring with low-cost GNSS sensors.



**Hongxing Zhang** received the Ph.D. degree from the Institute of Geodesy and Geophysics, Chinese Academy of Sciences, Wuhan, China, in 2019.

He is currently an Associate Professor with the Innovation Academy for Precision Measurement Science and Technology, Chinese Academy of Sciences. His research focuses on GNSS atmospheric remote sensing, atmospheric modeling, and precise positioning.



**Yunbin Yuan** is currently a Professor and the Director of the GNSS Research Group, Innovation Academy for Precision Measurement Science and Technology, Chinese Academy of Sciences, Wuhan, China. His research interests include GNSS-based spatial environmental monitoring and high-precision GNSS navigation and positioning.



**Matthias Aichinger-Rosenberger** received the Ph.D. degree from TU Wien, Vienna, Austria, in 2021.

He is currently a Post-Doctoral Scientist in space geodesy with ETH Zürich, Zürich, Switzerland. His main research interests are GNSS and their manifold applications for remote sensing (GNSS-RS), meteorology (data assimilation), and environmental monitoring.



**Benedikt Soja** received the Ph.D. degree from TU Wien, Vienna, Austria, in 2016.

He is currently an Assistant Professor of space geodesy with ETH Zürich, Zürich, Switzerland. His research focuses on GNSS data processing and machine learning applications in geodesy.